J. Fluid Mech. (1993), *vol.* 254, *pp.* 605–633

The hydraulics of steady two-layer flow over a fixed obstacle

By GREGORY A. LAWRENCE

Department of Civil Engineering, University of British Columbia, Vancouver, BC, Canada, V6T 1Z4

(Received 18 September 1992 and in revised form 18 February 1993)

This paper reports the results of a theoretical and experimental study of steady two-layer flow over a fixed two-dimensional obstacle. A classification scheme to predict the regime of flow given the maximum height of the obstacle, the total depth of flow, and the density and flow rate of each layer, is presented with experimental confirmation. There are differences between this classification scheme and that derived for flow over a towed obstacle by Baines (1984, 1987). These differences are due to the motion of upstream disturbances in towed obstacle flows. Approach-controlled flows, i.e. flows with an internal hydraulic control in the flow just upstream of the obstacle are studied in detail for the first time. This study reveals that non-hydrostatic forces, rather than a shock solution (called an internal hydraulic drop by previous investigators), need to be considered to explain the behaviour of Approach-controlled flows.

1. Introduction

This paper considers the steady, unidirectional flow of two layers of fluid of slightly different density over a fixed two-dimensional obstacle. To model tidally driven flows, or flows driven by large-scale pressure gradients in the atmosphere, barotropic forcing is assumed (i.e. sufficiently far upstream and downstream of the obstacle both layers move horizontally at the same speed). This study was motivated in part by the detailed observations of a remarkable variety of internal hydraulic phenomena in tidally driven flow over fjord sills by Farmer & Smith (1980), and Farmer & Freeland (1983). Motivation was also provided by a proposal of the US Army Corps of Engineers (1980) to build an underwater sill in Carquinez Strait to reduce the intrusion of saline water from San Francisco Bay through Carquinez Strait into the Sacramento–San Joaquin delta. For these cases variations in the flow are often negligible in the time it takes for fluid to pass over the sill, and the assumption of steady flow is warranted.

Considerable understanding of two-layer flow over an obstacle has been gained from towing-tank experiments, notably those of Long (1954) and Baines (1984). Two-layer towing-tank experiments are started with an obstacle at rest near one end of a tank containing two layers of immiscible fluid. The obstacle is then accelerated to a constant speed that is maintained until it approaches the other end of the tank. The intent is to create a steady flow in the neighbourhood of the obstacle while the obstacle is travelling at constant speed. In the flows of greatest interest, interfacial disturbances are generated that propagate upstream of the obstacle. It is worth considering the nature of these disturbances, since in many cases they result in the flow being unsteady in the neighbourhood of the obstacle throughout the experiment.

Baines (1984) has identified the three types of upstream disturbance depicted in figure 1. The nature of these disturbances is dependent upon the thickness of the lower

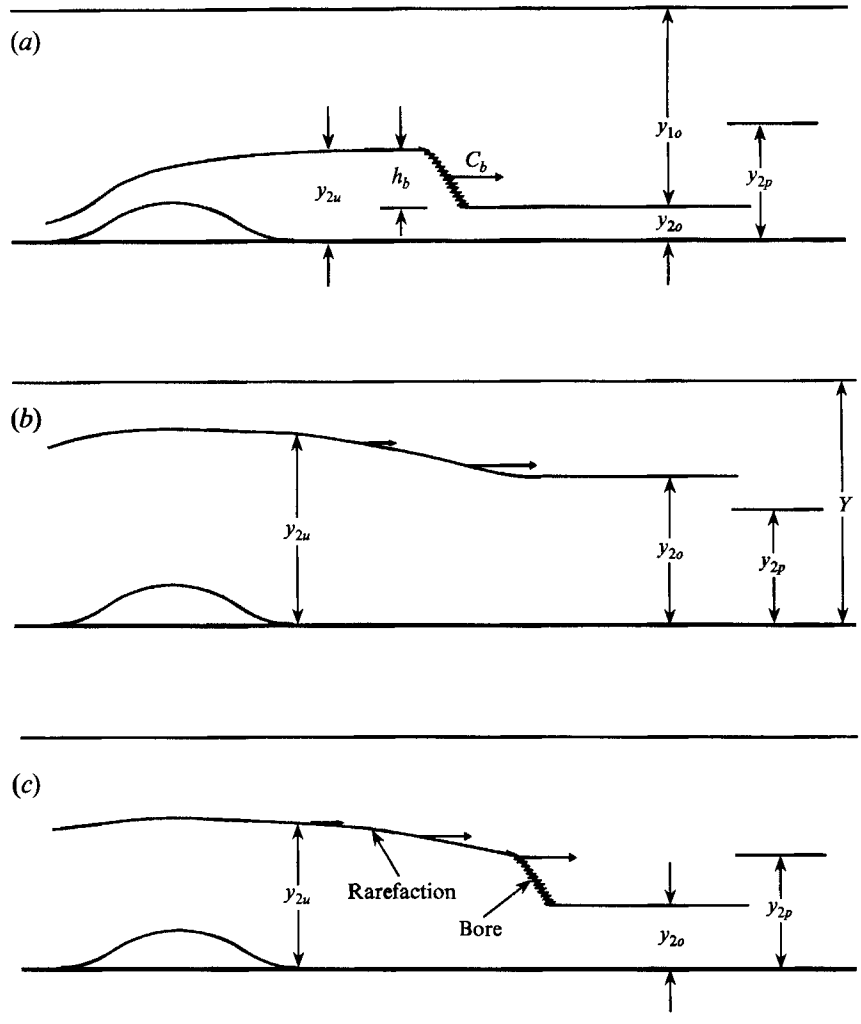

FIGURE 1. Examples of the three types of upstream disturbance generated in the towed-obstacle experiments of Baines (1984). The sketches are drawn in the frame of reference of the obstacle, which is being towed from left to right. (*a*) A bore (or moving hydraulic jump): an increase in propagation speed with increasing lower-layer thickness results in an internal bore moving upstream with velocity c_b. (*b*) A rarefaction (or negative wave): a disturbance that grows in length, since the leading portion of the disturbance travels faster than the trailing portion. (*c*) A combination of a bore and a rarefaction.

layer just upstream of the obstacle, y_{2u}, and the thickness of the lower layer far upstream of the obstacle, y_{2o}, which equals the initial thickness of the lower layer before the obstacle is set in motion. To a first approximation the internal phase speed of a disturbance at any location is proportional to the square root of the product of the upper- and lower-layer thicknesses at that location. Consequently, the phase speed peaks at a lower layer thickness, y_{2p}, that is approximately one-half the total depth, see Baines (1984). If $y_{2u} < y_{2p}$, as in figure 1(*a*), the increase in propagation speed with increasing lower-layer thickness will cause a steepening of the disturbance resulting in an internal bore which, in the absence of friction, moves upstream at a constant velocity, c_b, with respect to the obstacle. If $y_{2o} > y_{2p}$, as in figure 1(*b*), the disturbance will grow in length since, in this case, the thicker the lower layer the slower the

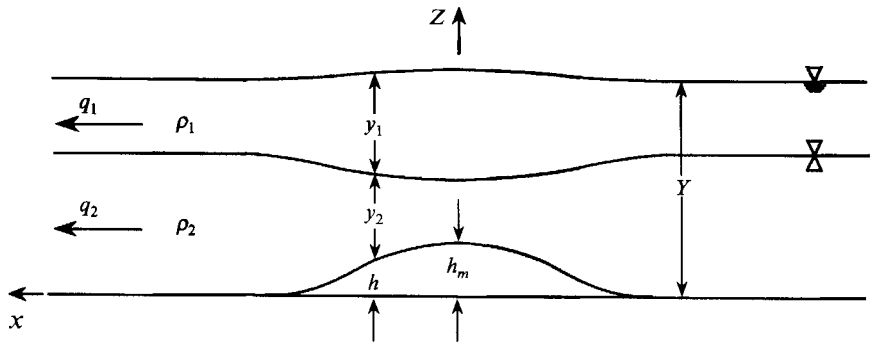

FIGURE 2. Definition diagram for steady two-layer flow over a fixed obstacle. The flow is drawn from right-to-left to correspond to the orientation of the photographs of the experiments.

propagation speed. The analogous phenomena is termed a 'negative wave' in open channel hydraulics (Henderson 1966); however, Baines (1984, 1987) adopts the term 'rarefaction' from gas dynamics. The third possibility, $y_{2u} > y_{2p} > y_{20}$, depicted in figure 1(*c*), is a combination of a bore and a rarefaction.

Consider the nature of the flow incident on an obstacle towed at constant velocity, U, in the presence of upstream disturbances. The simplest case is that of the upstream bore. Once the bore has formed, the flow is steady in the vicinity of the obstacle. In the reference frame of the obstacle the flow rates in the upper and lower layers upstream of the bore are $q_1^* = Uy_{10}$ and $q_2^* = Uy_{20}$, respectively, where y_{10} is the initial thickness of the upper layer. The flow rate of each layer in the vicinity of the obstacle must be adjusted to account for the motion of the bore; i.e. $q_1 = q_1^* + c_b h_b$, and $q_2 = q_2^* - c_b h_b$, where h_b is the height of the bore. For flows with rarefactions, steady flow in the vicinity of the obstacle can, in principle, still be achieved. However, Baines (1984, p. 156) reports that: 'In the regions where upstream rarefaction takes place, quantitative measurement of its magnitude was not possible because in most cases, the length of the tank was insufficient for the flow to reach steady state near the obstacle'. The results of Baines (1984) show that all upstream disturbances are rarefactions in flows with $r \geqslant 0.5$, where $r = y_{20}/Y$, and $Y = y_{10} + y_{20} + h$, is the total depth of fluid. For $r < 0.5$ some upstream disturbances are rarefactions. Therefore, the towed obstacle technique may not be an effective means of investigating steady flows, especially if $r \geqslant 0.5$. For this reason Baines (1984) concentrates on flows with $r \leqslant 0.5$.

To study steady two-layer flow over an obstacle it is most effective to fix an obstacle to the bottom of a flume and to allow two fluids of different density to flow over it at a constant rate, as depicted in figure 2. In the present study fresh and salt water were used, and a steady flow, devoid of any bores or rarefactions, was maintained for several hours at a time. Section 3 of this paper describes how the experimental facility was configured to ensure that, without the obstacle in place, both layers have the same velocity. This provides an initial, or undisturbed, flow analogous to the towed obstacle experiments we can write

$$r = y_{20}/Y = q_2/q, \tag{1}$$

where $q = q_1 + q_2$, and q_1 and q_2 are the two-dimensional flow rates for the upper and lower layers, respectively. The fixed-obstacle approach also has the advantage of being more convenient for gathering data, since probes and visualization equipment do not have to be towed down the tank with the obstacle. The use of miscible fluids also permitted a study of mixing between the layers, the results of which will be presented

in a subsequent paper. Neither towed-obstacle nor fixed-obstacle experiments accurately represent all the important features of natural flows. Rather, they place useful bounds on the range of expected behaviour, and should be regarded as providing complementary rather than conflicting information.

The objectives of this study are to identify and investigate the nature of the basic regimes of steady two-layer flow over an obstacle in greater detail than has been possible in towed obstacle experiments, and to develop a classification scheme to predict, for any given set of conditions, which regime will occur. A review of internal hydraulic theory is presented §2. Section 3 provides a description of the experimental apparatus and procedures. The derivation of the classification scheme is given in §4. Section 5 provides a comparison of theoretical predictions with laboratory and field observations. Conclusions are presented in §6.

2. Basic internal hydraulic theory

A brief summary of internal hydraulic theory is presented in this section. Readers interested in more detailed accounts are referred to the papers of Baines (1984, 1987), Armi (1986), and Lawrence (1990). The present study considers the steady, unidirectional two-layer flow of an incompressible fluid over an isolated two-dimensional obstacle, located in an otherwise horizontal channel of constant width, see figure 2. A series of assumptions will be presented that simplify the equations of motion. Although there are a number of circumstances where one or more of these assumptions is violated, the resulting equations accurately describe many of the features of two-layer flow over an obstacle.

We begin by assuming that there is *no mixing* so that the density along a streamline, ρ_s, is constant. With the second assumption of *inviscid* flow the equations of motion become

$$-\frac{1}{\rho_s}\frac{\partial P^*}{\partial s} = \frac{\partial (v^2/2)}{\partial s}, \tag{2}$$

and

$$-\frac{1}{\rho_s}\frac{\partial P^*}{\partial n} = \frac{v^2}{r_c}, \tag{3}$$

where s is the streamwise direction, n is the direction normal to the streamline passing through its center of curvature, r_c is the radius of curvature of the streamline, and v is the fluid velocity. Lawrence (1984) and Jirka (1984) have demonstrated that it is the piezometric pressure, $P^* = P + \rho_s gz$, not the pressure P, that is of primary importance in the study of internal hydraulics, where g is the gravitational acceleration, and z is elevation above the horizontal bed of the channel.

If the sill is 'gentle', that is, if its minimum radius of curvature is much greater than its height, it is customary (see Long 1954) to make a third assumption, called the *hydrostatic* assumption, that $\partial P^*/\partial n = 0$. Cases where non-hydrostatic pressures are important even when the sill is gentle will be discussed in §5, but for the moment hydrostatic pressure is assumed. The fourth assumption is that if the maximum sill slope is small, then the streamlines will be essentially horizontal and the flow is *one-dimensional*. In this case we can replace s by x, and v by u, where x and u are the horizontal direction and velocity, respectively.

We make a fifth assumption that the flow is *layered*, and that within each layer the density is constant and the velocity varies only in the flow direction. So we set $u_n = q_n/y_n$, where the velocity, two-dimensional flow rate, and thickness of each layer

are denoted by u_n, q_n, and y_n respectively, with $n = 1$ for the upper layer and $n = 2$ for the lower layer. With the above assumptions the piezometric pressure is constant within each layer, and given by

$$P_1^* = \rho_1 g(y_1 + y_2 + h), \tag{4a}$$

and

$$P_2^* = \rho_1 g y_1 + \rho_2 g(y_2 + h), \tag{4b}$$

where h is the height of the obstacle. If the above assumptions hold then

$$\mathrm{d}E_n/\mathrm{d}x = 0, \tag{5a}$$

where

$$E_n \equiv P_n^* + \tfrac{1}{2}\rho_n u_n^2 \tag{5b}$$

is the Bernoulli constant (mechanical energy per unit volume). Equations (4) and (5) can be rewritten in the form

$$\boldsymbol{A}\frac{\mathrm{d}\boldsymbol{b}}{\mathrm{d}x} = \frac{\mathrm{d}\boldsymbol{c}}{\mathrm{d}x}, \tag{6}$$

where

$$\boldsymbol{A} = \begin{bmatrix} 1-\epsilon F_1^2 & 1 \\ 1-\epsilon & 1-\epsilon F_2^2 \end{bmatrix}, \quad \boldsymbol{b} = \begin{bmatrix} y_1 \\ y_2 \end{bmatrix}, \quad \boldsymbol{c} = \begin{bmatrix} -h \\ -h \end{bmatrix}.$$

The densimetric Froude numbers of the individual layers are denoted by $F_n^2 = u_n^2/g' y_n$, where the reduced gravitational acceleration, $g' = \epsilon g$, and the relative density difference, $\epsilon = (\rho_2 - \rho_1)/\rho_2$. Solving (6) for y_1 and y_2, and noting that the free-surface elevation, $Y = y_1 + y_2 + h$, gives

$$\frac{\mathrm{d}Y}{\mathrm{d}x} = \frac{\epsilon F_1^2 F_2^2}{1 - G^2}\frac{\mathrm{d}h}{\mathrm{d}x}, \tag{7}$$

where the composite internal Froude number, $G^2 = F_1^2 + F_2^2 - \epsilon F_1^2 F_2^2$. Lawrence (1990) has shown that even though the composite Froude number is not a Froude number in the strictest sense (it is not the ratio of a convective velocity to a long-wave phase speed), it correctly specifies the criticality of the flow; i.e. if $G^2 < 1$ the flow is internally subcritical, if $G^2 = 1$ it is internally critical and if $G^2 > 1$ it is supercritical.

The sixth assumption is the *Boussinesq* assumption that $\epsilon \ll 1$. In the present study we shall only deal with flows with $F_n^2 = O(1)$, so that from (7) we can make the seventh assumption of a *horizontal free surface*. With this assumption attention can be focused on the variation in interface height, which, from (6) and the Boussinesq approximation, is given by

$$\frac{\mathrm{d}\eta}{\mathrm{d}\chi} = -\frac{F_2^2}{1 - G^2}\frac{\mathrm{d}\beta}{\mathrm{d}\chi}, \tag{8}$$

where lengthscales normalized with respect to Y have been used, i.e. the dimensionless horizontal distance $\chi \equiv x/Y$, the dimensionless obstacle height, $\beta \equiv h/Y$, and the dimensionless interfacial deflection, $\eta \equiv (h + y_2 - y_{20})/Y$. Using (1) we obtain $\eta = \beta + y_2/Y - r$.

Any location where $G^2 = 1$ is customarily called a control, and is of importance since to avoid an interface slope (8) requires that $\mathrm{d}\beta/\mathrm{d}x = 0$. Thus a control can only occur either at the crest of the obstale, or in the horizontal channel upstream or downstream of the obstacle. If a control location is known, then the condition $G^2 = 1$ is used in conjunction with the requirement that the flow passes from subcritical to supercritical

at a control, to determine the interface height at the control. L'Hôpital's rule must then be applied to obtain the interfacial slope at the control; i.e.

$$\frac{\mathrm{d}\eta}{\mathrm{d}\chi} = \pm\left(\frac{-F_2^2\,\mathrm{d}^2\beta/\mathrm{d}\chi^2}{3[F_2^2/(r+\eta-\beta)-F_1^2/(1-r-\eta)]}\right)^{\frac{1}{2}}. \tag{9}$$

The sign in front of the square root is chosen to ensure transition from subcritical to supercritical flow at the control. Finally (8) is used to determine the variation in interfacial elevation both upstream and downstream of the control, see §5.2.

An alternative to the above procedure is to define a dimensionless internal energy:

$$E \equiv \frac{E_2 - E_1}{\rho_2 g' Y} - r. \tag{10}$$

The flow rate ratio, r, has been included in this definition to ensure that, if $u_1 = u_2$, then from 5(b), $E = 0$. So the dimensionless internal energy becomes a measure of the deviation of the flow from the assumed undisturbed state in which $u_1 = u_2$. Given (6) and (10) and the horizontal-free-surface assumption we can write

$$\frac{\mathrm{d}E}{\mathrm{d}\chi} = 0. \tag{11}$$

This result is fundamental to internal hydraulic theory, but is only valid when the seven assumptions listed above are satisfied. If one or more of these assumptions is violated, as is the case in internal hydraulic jumps and regions of flow separation, then (11) does not hold. Substituting from (6), and using the horizontal-free-surface and Boussinesq assumptions, gives

$$E = \eta + \tfrac{1}{2}r(1-r)\,G_0^2\left\{\left[\frac{r}{(r+\eta-\beta)}\right]^2 - \left[\frac{(1-r)}{(1-r-\eta)}\right]^2\right\}, \tag{12}$$

where the undisturbed composite Froude number, $G_0^2 = q^2/\{g'r(1-r)\,Y^3\}$. For the flows considered in this paper G_0^2 and r are fixed so that once the internal energy is known at a point of control, (11) can be solved to obtain η as a function of the β.

Several investigators, including Lawrence (1985), Farmer & Denton (1985), Denton (1987) and Dalziel (1990), have recognized that

$$\partial E/\partial\eta = 1 - G^2 \tag{13}$$

and made use of (E, η)-curves to represent two-layer flows. Two such curves for a flow with $r = 0.5$, and $G_0 = 0.5$ are presented in figure 3. In the first, with $\beta = 0.5$, η is a monotonically decreasing function of E and (13) tells us that the flow must be supercritical no matter what the position of the interface. From Lawrence (1985, Appendix C) this only occurs if and only if

$$G_0^2 > \frac{(1-\beta)^3}{r(1-r)\,[r^{\frac{1}{2}} + (1-r)^{\frac{1}{2}}]^4}. \tag{14}$$

If the inequality is reversed in (14), as in the second case with $\beta = 0$, there are values of E for which there are three possible interface positions: one corresponding to supercritical flow with a thin upper layer; one corresponding to supercritical flow with a thin lower layer; and one corresponding to subcritical flow. The (E, η)-curves help us predict which of the three possible interface positions will occur. Such curves are

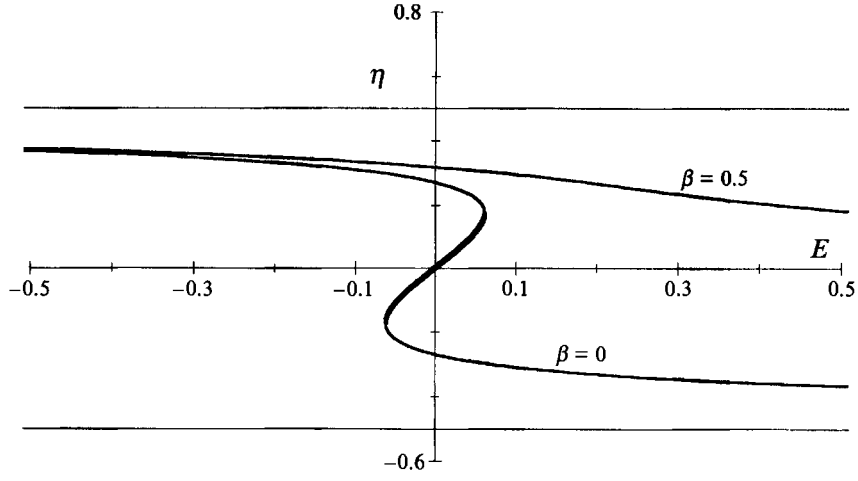

FIGURE 3. The (E, η)-curves for $\beta = 0$ and $\beta = 0.5$ in a flow with $r = 0.5$ and $G_0 = 0.5$. ——, supercritical flow since $\partial E/\partial \eta < 0$; ——, subcritical flow since $\partial E/\partial \eta > 0$.

similar to energy curves used in Lawrence's (1987) analysis of single-layer flows. However, it must be emphasized that the internal energy for two-layer flows is analogous to the total (not specific) energy of single-layer flows.

The (E, η)-curves are not the only way of graphically representing two-layer flows, for example Armi (1986) presents essentially the same information on a Froude number plane. The (E, η) approach has been chosen for use in the present study to clearly show variations in internal energy and to provide direct comparisons with photographs of the experiments. In addition they are used extensively in the derivation of the classification scheme for steady two-layer flow over a fixed obstacle in §4. Before presenting this derivation the experimental design and procedures need to be discussed.

3. Experimental design and procedures

The experimental facility was designed to produce a sustainable, steady two-layer flow over a two-dimensional obstacle. The intent was to allow a more effective study of steady flows than is possible in towing-tank experiments. Figure 4(*a*) is a photograph of an experiment in progress. A steady two-layer flow of fresh (clear) water and saline (dyed) water is flowing from right to left over a fixed obstacle, see figure 4(*b*).

The plan view of the facility (figure 4*c*) shows that the flow first passes through a fixed contraction, then through a constant-width flume (the test section), and finally through an adjustable downstream contraction. This configuration was specifically chosen to model barotropically driven flows, since, for inviscid, Boussinesq flows, Wood's (1968) result shows that when there is no obstacle, both layers will have the same velocity throughout the facility. When the flow is subcritical in the test section, i.e. $G_0^2 < 1$, an internal hydraulic control (called a 'virtual control' by Wood 1968) will be located in the downstream contraction. Placing an obstacle in the test section may add an additional control in the vicinity of the obstacle, but will not affect the virtual control. If the flow is supercritical in the test section, i.e. $G_0^2 > 1$, then a virtual control will be located in the upstream contraction. The presence of an obstacle within the test section will not, in general, add an additional control, it will merely cause the flow to become more highly supercritical as it passes over the obstacle. These results are crucial to the development of the classification scheme presented in §4.

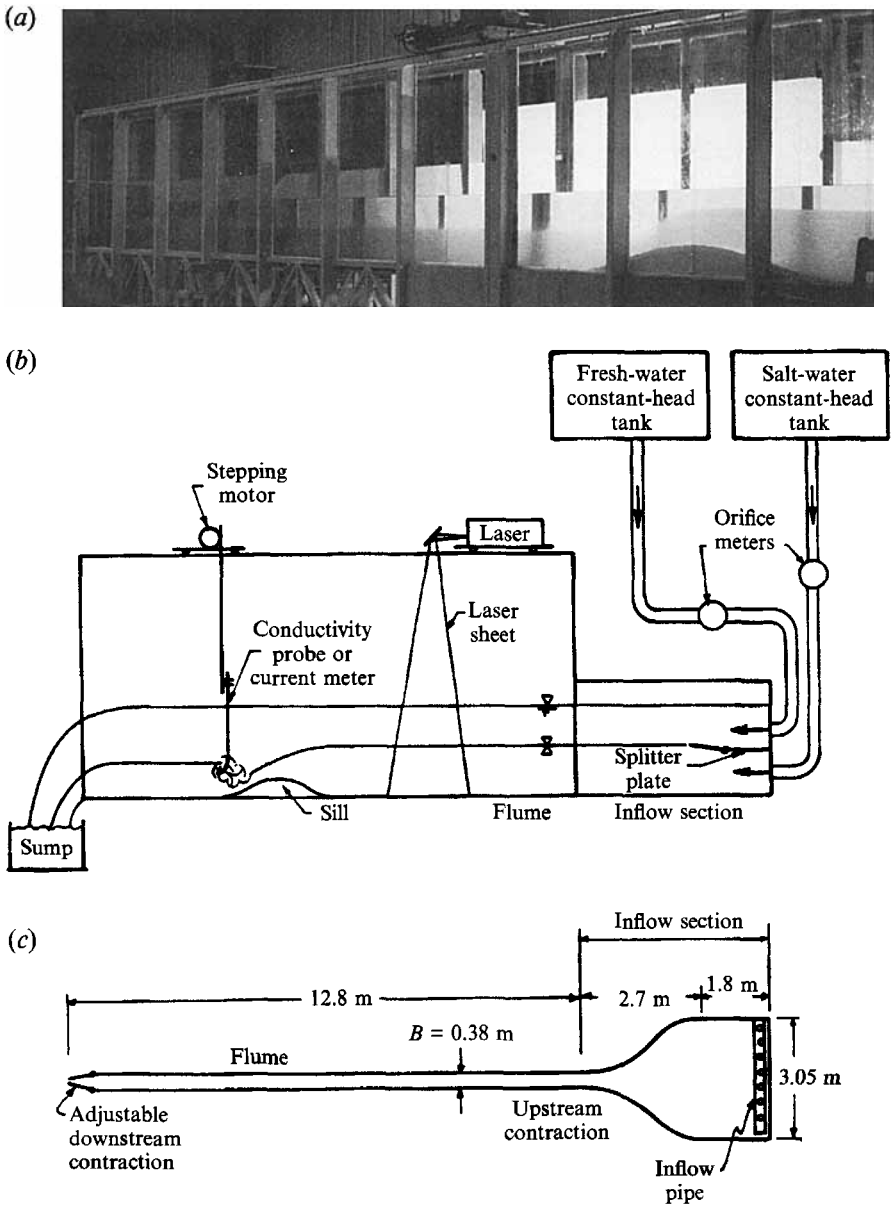

FIGURE 4. The experimental setup: (*a*) a view of an experiment in progress (looking downstream): (*b*) side view: (*c*) plan view.

The details of the experimental set-up can be explained with the help of the side view given in figure 4(*b*). Fresh water from the mains supplies one constant-head tank, and salt water drawn from San Francisco Bay into a 370 m^3 pond supplies the other. The maximum discharge from each of these head tanks is 10^{-2} m^3/s, so the experiment can be run at maximum flow for 10 hours before the salt water pond is emptied. The basic experimental data for each of the 25 experiments are listed in table 1. The discharges are measured to within $\pm 2\%$ by a pair of orifice meters. The total two-dimensional discharge varied between 0.007 and 0.05 m^2/s. Thus, defining Reynold's number,

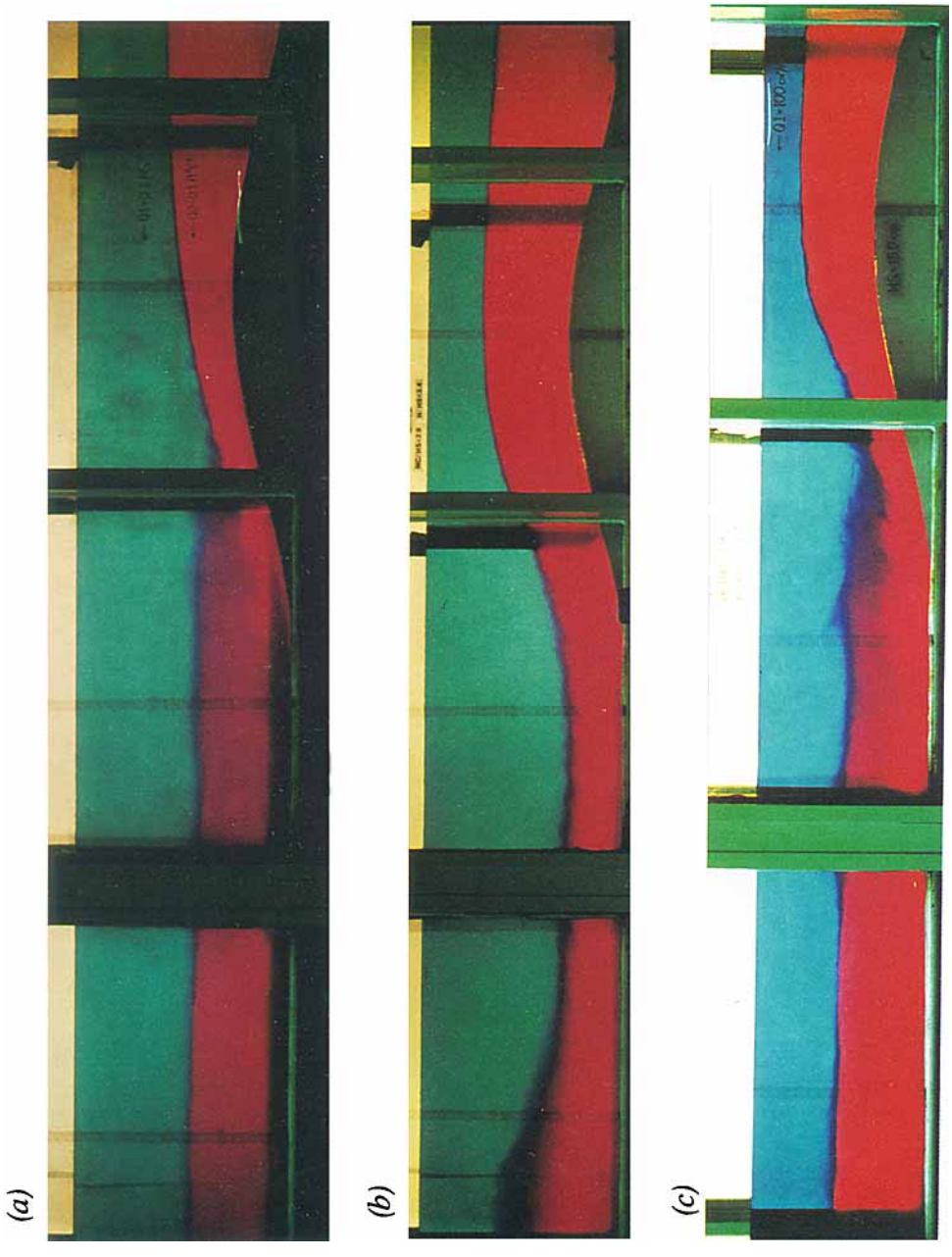

FIGURE 6. Photographs of a Crest-controlled flow (*a*) experiment 15; and two Approach-controlled flows (*b*) experiment 21, and (*c*) experiment 17. Flow is from right to left in each case. The upper (fresh) layer is dyed blue, and the lower (saline) layer is dyed red. When the two layers mix an intermediate (purple) layer forms.

Exp.	Y (cm)	q_1 (cm^2/s)	q_2 (cm^2/s)	g' (cm/s^2)	r	b_m	G_0	Regime	Figure
1	43.8	23	47	17.9	0.67	0.34	0.12	I	7(*a*)
2	38.1	43	86	20.4	0.67	0.39	0.26	II	11
3	51.4	57	112	5.7	0.66	0.29	0.41	II	—
4	46.8	57	112	5.6	0.66	0.32	0.47	II	7(*b*)
5	30.5	24	47	5.9	0.66	0.49	0.36	II/III	16
6	26.5	23	46	5.9	0.66	0.57	0.44	III	17
7	39.2	57	112	5.5	0.66	0.38	0.62	III	7(*c*)
8	36.3	57	112	5.6	0.66	0.41	0.69	III	—
9	32.1	57	112	5.6	0.66	0.47	0.83	III	—
10	30.2	57	112	5.7	0.66	0.50	0.90	III/IV	—
11	28.4	57	112	5.9	0.66	0.53	0.97	IV	—
12	25.7	100	200	17.9	0.67	0.58	1.15	IV	19
13	56.7	101	101	8.4	0.50	0.26	0.32	II	—
14	35.9	72	72	14.0	0.50	0.42	0.36	II	—
15	51.4	101	101	7.9	0.50	0.29	0.39	II	6(*a*)
16	32.0	72	72	13.4	0.50	0.47	0.44	III	—
17	40.2	101	99	8.0	0.49	0.37	0.55	III	6(*c*)
18	39.4	145	145	12.8	0.50	0.38	0.66	III	—
19	46.5	204	204	14.8	0.50	0.32	0.67	III	—
20	46.2	249	249	18.4	0.50	0.32	0.74	III	—
21	51.1	204	205	8.8	0.50	0.29	0.75	III	6(*b*)
22	44.1	204	204	8.9	0.50	0.34	0.93	III/IV	—
23	41.4	204	204	8.9	0.50	0.36	1.02	IV	7(*d*)
24	26.2	101	101	7.5	0.50	0.57	1.10	IV	—
25	43.8	34	94	7.5	0.74	0.34	0.37	I	10

TABLE 1. Experimental data. *Note*: The maximum height of the obstacle is 15 cm in all experiments

$Re = q/\nu$, yields values varying between 7000 and 50000, which are higher than most laboratory experiments. Pipes leading from the constant-head tanks discharge fluid evenly across the width of the inflow section. The splitter plate installed between these pipes was hinged so that its trailing edge could be set at the height of the interface in the flow section to minimize mixing between the two fluids.

In some of the experiments velocity and density profiles were measured at a limited number of locations using a miniature propeller meter and a conductivity probe. Details of the instrumentation are given in Lawrence (1985). However, in most cases the interface level was visualized by colouring one or both of the layers with dye. The velocity and density measurements for experiment 21 are plotted in figure 5 together with the visual measurements of the interface level. Upstream of the obstacle the density interface is about 1 cm thick and visual observations of interface level are accurate to within about ± 3 mm. As the flow passes over the obstacle, the lower layer accelerates, and the shear across the interface generates instabilities and mixing between the two layers. This can be seen in figure 6 (plate 1) where the blue and red dyes of the upper and lower layers mix to form a purple interfacial region. Once significant mixing has occurred visual observations of the interface level are less reliable. However, this is of no great concern since the interface position in regions of the flow where mixing is minimal are of greatest interest in the present study.

The density of each fluid was measured in the inflow section using a hydrometer that enabled the relative density difference to be determined to within ± 0.0003. The relative density differences used were in the range $0.0057 < \epsilon < 0.0209$. The glass-sided flume

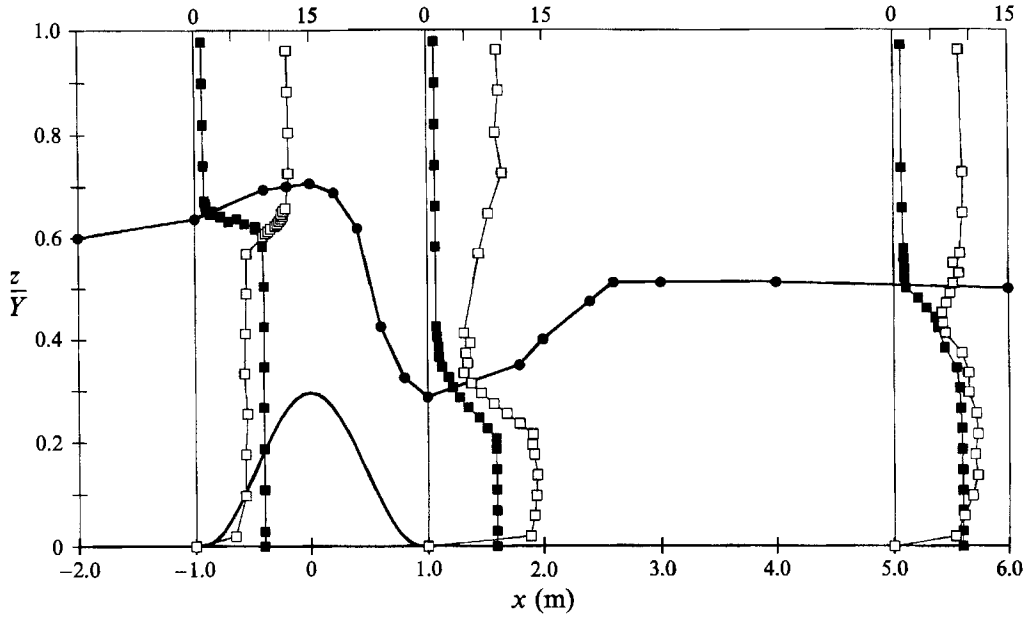

FIGURE 5. Density (■) and velocity (□) profiles at $x = -1.0$ m, 1.0 m, and 5.0 m in experiment 21 plotted together with visual observations of interface position. Density is measured in σ_t units, where $\rho(\sigma_t) = \rho(\text{kg/m}^3) - 1000$, and velocity in cm/s. Flow is from left to right.

is 12.8 m long, 37.6 cm wide, and the depth of flow varied from 25.7 cm to 56.7 cm over the series of experiments. Since the relative density difference $\epsilon \ll 1$ there is essentially no longitudinal variation of the free-surface elevation within the test section. The free-surface elevation was controlled by varying the width of the downstream contraction. Variations in the inflow rates caused the free surface to fluctuate about ± 1 mm. The measurement error was about ± 1 mm.

The obstacle shape satisfies the equation

$$h(x) = h_m \cos^2(x/L) \tag{15}$$

to within ± 2 mm over the range $|x/L| \leqslant \frac{1}{2}\pi$, where the maximum height of the obstacle, $h_m = 150$ mm, and the lengthscale $L = 4h_m$. The cosine squared function was chosen, since for a given length and height of the obstacle, the maximum values of obstacle slope and curvature are relatively low when compared with other possible obstacle shapes.

4. Classification scheme

It was found experimentally, and will be shown theoretically, that there are four basic regimes of steady two-layer flow over a fixed two-dimensional obstacle. These regimes are shown in figure 7, which presents photographs of experiments representing each of the four regimes alongside the corresponding (E, η)-curves. In Regime I (Subcritical flow) the flow is subcritical everywhere with the obstacle causing a slight depression in the interface level, see figure 7(*a*). In Regime II (Crest-controlled flow) the flow passes from subcritical to supercritical at the crest of the obstacle, and then becomes subcritical again downstream of an internal hydraulic jump, see figure 7(*b*). For Regime III (Approach-controlled flow) the flow passes from supercritical to

subcritical just before the start of the obstacle, and like Crest-controlled flow becomes subcritical again downstream of an internal hydraulic jump, see figure 7(*c*). In Regime IV (Supercritical flow) the flow is supercritical everywhere with the interface rising as the flow passes over the sill, see figure 7(*d*). Regimes I, II, and IV have direct counterparts in single-layer (open channel) flow, and the variation in interface level is analogous to the variation in free-surface level in single-layer flows. On the other hand, Regime III (Approach-controlled flow) is new and has no counterpart in single-layer flow. It has several unique features that will be discussed below.

For steady two-layer flow over a fixed obstacle there are five important variables: Y, h_m, g', q_1, q_2. From these variables the following three non-dimensional parameters can be formed to specify any particular flow: the flow rate ratio, $r = q_2/q$; the non-dimensional maximum obstacle height, $\beta_m = h_m/Y$; and the undisturbed composite Froude number, $G_0 = q/(g'r(1-r)\,Y^3)^{\frac{1}{2}}$. The values of these parameters for the experiments discussed in this paper are listed in table 1. The classification scheme provides, for a given r, diagrams indicating regions of the (β_m, G_0)-plane corresponding to each of the flow regimes.

For a given set of basic parameters (r, β_m, and G_0) the (E, η)-curve only changes as the flow passes over the obstacle; i.e. as β changes. Of primary concern are the (E, η)-curves for $\beta = 0$ and β_m, referred to as the channel and crest curves respectively. For a large range of parameters these curves have both a local maximum and a local minimum in E. The local minimum of the crest curve, denoted E_c, is the internal energy at the crest in a Crest-controlled flow, see figure 7(*b*). In figure 7(*c*) we see that a control can occur in the flow as it approaches the obstacle. At this 'approach-control' the internal energy is the local maximum of the channel curve, E_a.

To make use of the (E, η)-curves we must be able to predict the value of E. Wood's (1968) result that $u_1 = u_2$ at a virtual control in a Boussinesq flow yields $E = 0$, a condition that would hold throughout the channel if all the assumptions made in §2 were satisfied. Typically they are not. Significant amounts of energy are dissipated (primarily in the lower layer) in an internal hydraulic jump, resulting in a drop in internal energy; in addition, streamline curvature as the flow passes over the obstacle causes significant variations in E, see figures 7(*b*) and 7(*c*). Smaller variations in E can arise from violations of the one-dimensional assumption that within each layer the density is constant and the velocity varies only in the flow direction. Vertical variations in velocity and density within the layers in experiment 21 are shown clearly in figure 5. Upstream of the obstacle the flow is distinctly two layered, but downstream of the crest the velocity profiles become complicated by the presence of the internal hydraulic jump, and the density interface thickens as a result of mixing between the layers, see figure 6 also.

The drop in E across the internal hydraulic jump is incorporated into the classification scheme; however, incorporation of other variations in internal energy would complicate the classification scheme so much as to make it unusable. For the purpose of deriving the classification scheme it is assumed that, if there is an internal hydraulic jump in the flow, then E is constant and greater than zero upstream of it and equal to zero downstream of it. In the absence of an internal hydraulic jump E is assumed to be equal to zero everywhere.

We can now construct the classification scheme. Regime I (Subcritical flow) occurs when $E_c < 0$, and Regime II (Crest-controlled flow) occurs when $0 < E_c < E_a$, see figures 7(*a*) and 7(*b*). The remainder of the classification scheme is determined by the fact that, when there is no obstacle, if $G_0^2 > 1$, then the flow is supercritical throughout

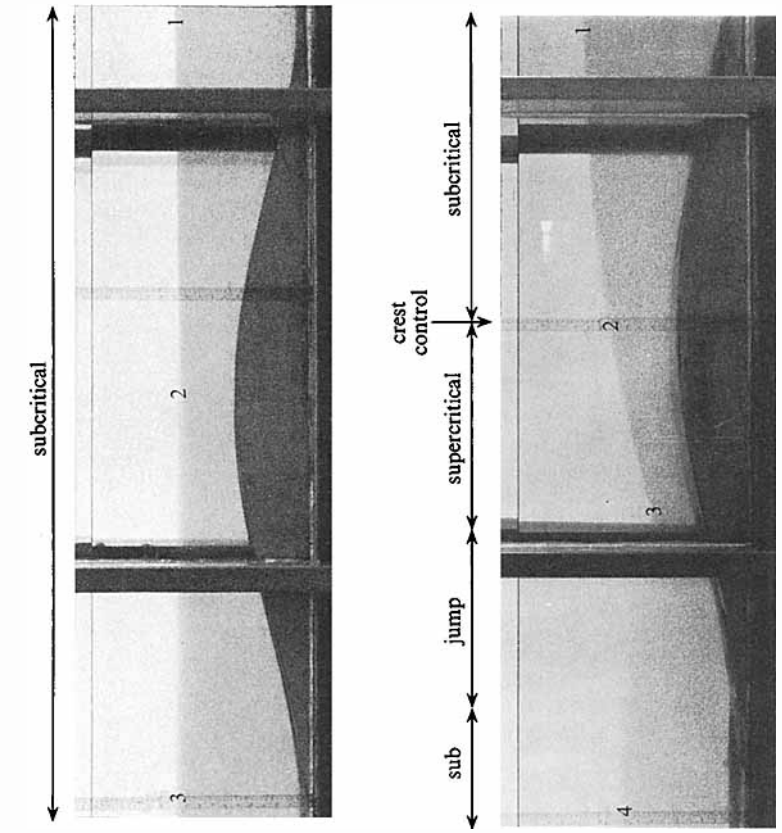
subcritical
1
2
3
crest control
subcritical
supercritical
jump
sub
1
2
3
4

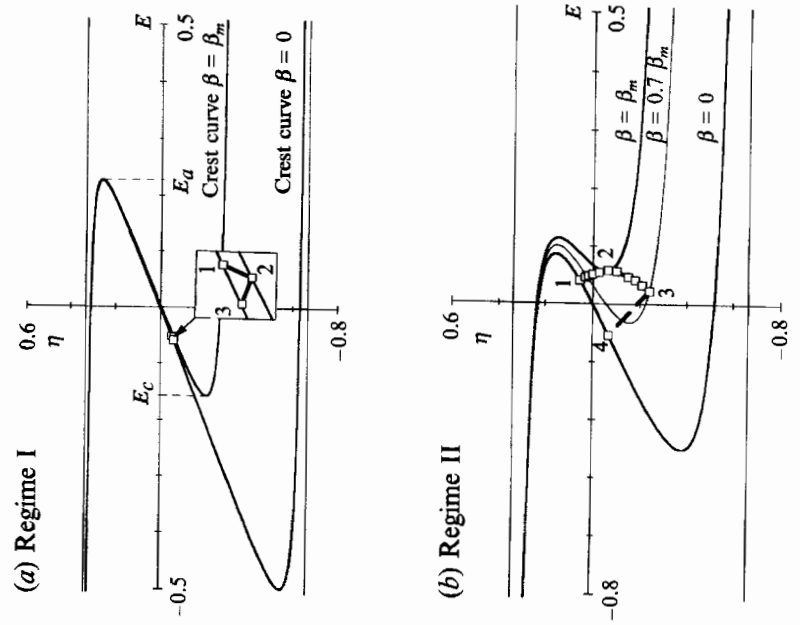
(a) Regime I
0.6
η
E
0.5
E_a
Crest curve $\beta = \beta_m$
Crest curve $\beta = 0$
E_c
−0.5
−0.8
1
2
3
(b) Regime II
0.6
η
E
0.5
$\beta = \beta_m$
$\beta = 0.7\,\beta_m$
$\beta = 0$
−0.8
1
2
3
4

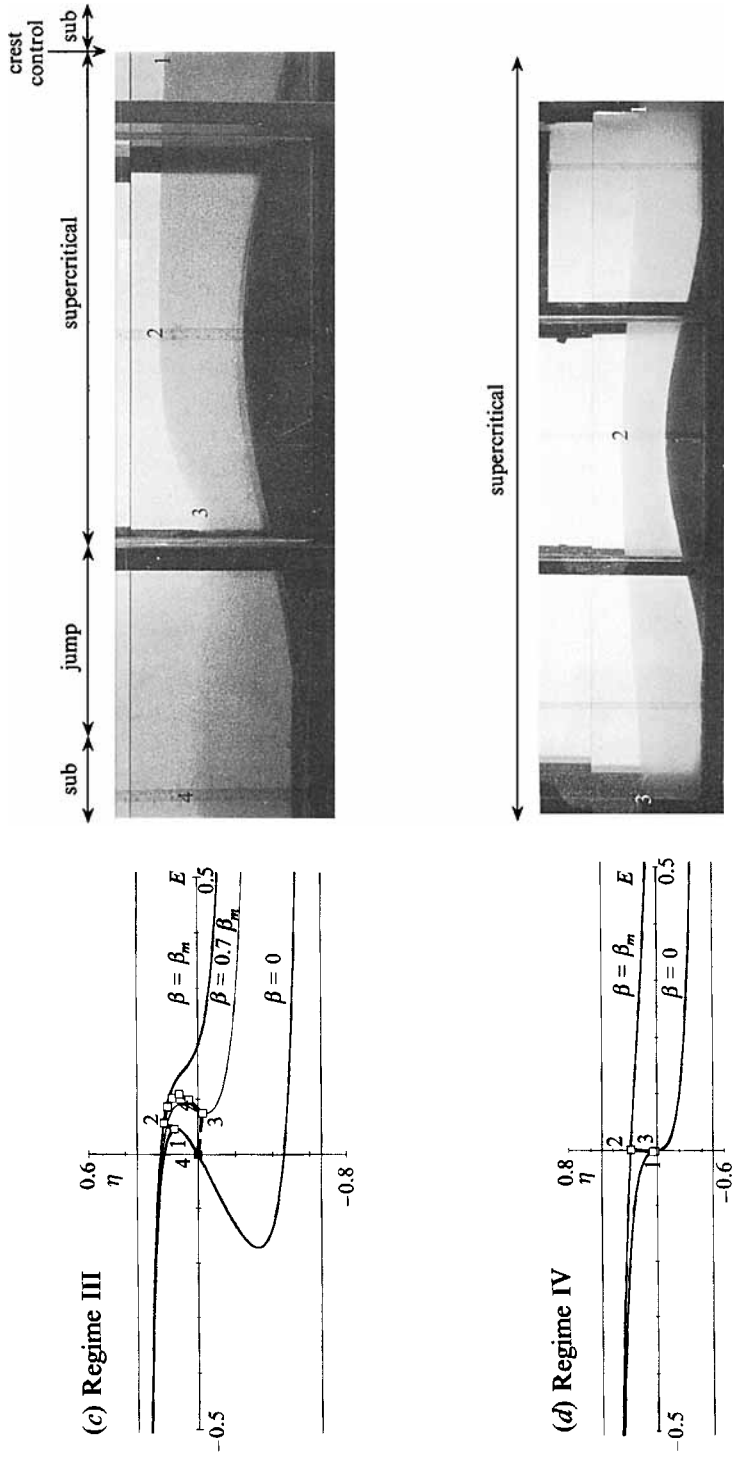

FIGURE 7. Internal energy diagrams and photographs of flows typical of each of the flow regimes. Flow is from right to left in each case. The open squares represent experimental measurements of interface level. (*a*) Experiment 1, an example of Regime I (Subcritical flow) characterized by internally subcritical flow in the vicinity of the obstacle. (*b*) Experiment 4, an example of Regime II (Crest-controlled flow) characterized by internally subcritical flow upstream of the crest, critical flow at the crest, and supercritical flow immediately downstream of the crest, followed by an internal hydraulic jump. (*c*) Experiment 7, an example of Regime III (Approach-controlled flow) characterized by internally subcritical flow upstream of the obstacle, critical flow near the foot of the obstacle, and supercritical flow over the obstacle, followed by an internal hydraulic jump. (*d*) Experiment 23, an example of Regime IV (Supercritical flow) characterized by internally supercritical flow in the vicinity of the obstacle.

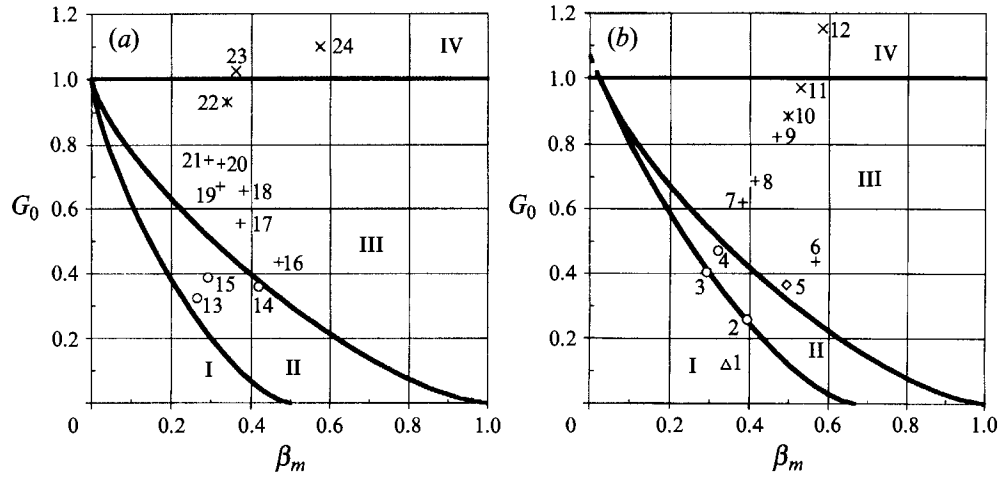

FIGURE 8. Classification diagrams for (*a*) $r = \frac{2}{3}$, and (*b*) $r = \frac{1}{2}$. The points represent each of the experiments. △, Regime I: Subcritical flows; ○, Regime II: Crest-controlled flows; ◇, Hybrid flows exhibiting features of both Regimes II and III; +, Regime III: Approach-controlled flows; ×, Hybrid flows exhibiting features of both regimes III and IV, ×, Regime IV: Supercritical flows.

the test section. With an obstacle in place there are two alternatives. The first, and most common, is that the flow remains supercritical throughout the test section, the only change being an increase in the Froude number over the obstacle, so Regime IV (Supercritical flow) can occur whenever $G_0^2 > 1$. The second alternative is that when $0 < E_c < E_a$ and $G_0^2 > 1$ there is the possibility of a jump upstream of the obstacle followed by a crest-controlled flow. This alternative has been investigated for the towed-obstacle case for very small values of r by Baines (1984), and for single-layer flow by Lawrence (1987), but will not be pursued in the present study. Solutions to the equations $E_c = 0$, $E_c = E_a$, and $G_0^2 = 1$ have been plotted on the (β_m, G_0)-plane, for $r = \frac{1}{2}$ and $\frac{2}{3}$, in figures 8(*a*) and 8(*b*). The regions of these classification diagrams associated with each of the flow regimes are readily apparent.

The points corresponding to the experiments performed in the present study are plotted on figure 8. These experiments verify the classification scheme, although four experiments need to be commented on. Experiment 5 falls close to the boundary between Regimes II and III and combines features of both those regimes; similarly experiments 10 and 22 fall close to the boundary between Regimes III and IV, and combine features of both those regimes. These hybrid flows will be discussed further in §5.3. Experiment 11 is the only experiment that appears to violate the classification scheme. However, of all the experiments, experiment 11 has one of the lowest relative density differences and one of the lowest total depths of flow. Accounting for experimental error gives $G_0 = 0.97 \pm 0.05$, so it is not altogether surprising that experiment 11 behaves as if it were a Supercritical flow with $G_0 > 1.0$.

The success of the classification scheme deserves some comment, since there are several important sources of variation in internal energy, including friction and streamline curvature, that have been ignored. Fortunately, these variations are generally not significant in the vicinity of internal hydraulic controls. For instance, there is significant variation in internal energy in Crest-controlled flows, but $\mathrm{d}E/\mathrm{d}x \approx 0$ at the crest, see figure 7(*b*). So, although internal energy variations are

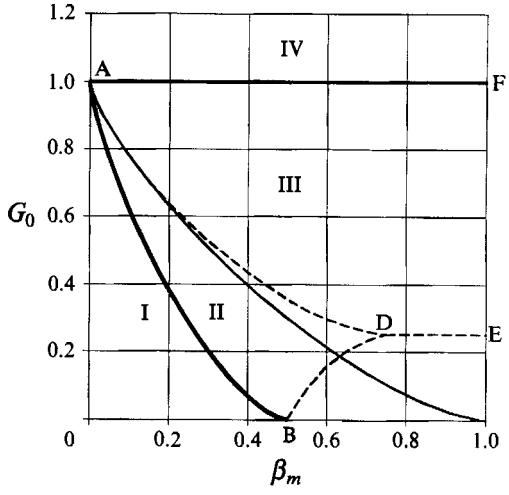

FIGURE 9. Comparison of classification schemes for $r = \frac{1}{2}$ of Baines (1987) for towed-obstacle flows with that of the present scheme for fixed-obstacle experiments. ——, Curves common to both schemes, curve AB separates Regime I (Subcritical flow) from Regime II (Crest-controlled flow), and curve AF separates Regime III (Approach-controlled flow) from Regime IV (Supercritical flow). ——, Curve AC is found only in the fixed-obstacle scheme of the present paper and separates Regime II (Crest-controlled flow) from Regime III (Approach-controlled flow). – – –, Curves AD, BD, and DE are all associated with flows with upstream rarefactions and are therefore only found in the towed-obstacle scheme of Baines (1987, figure 5).

important in determining the details of the flows, they have little effect on the position of the internal hydraulic controls, and the classification scheme is still effective.

4.1. *Comparison with classification scheme of Baines* (1987)

The classification scheme for $r = 0.5$ is plotted together with the scheme of Baines (1987, figure 5) in figure 9. The notation is slightly different: Baines (1987) uses F_0 rather than G_0, and H rather than β_m. As in the case of single-layer flows, see Lawrence (1987), the classification schemes for towed-obstacle and fixed-obstacle flows are different. Curves AD, BD, and DE are all associated with flows with upstream rarefactions and are therefore only found in the towed-obstacle scheme of Baines (1987). Curve AC is found only in the fixed-obstacle scheme of the present paper and separates Crest-controlled flow from Approach-controlled flow. The bounds on the Subcritical and Supercritical flow regimes are the same in both schemes, since there are no upstream disturbances associated with these regimes.

5. Experimental results and discussion

In this section quantitative comparisons are made between experimental measurements and the predictions of internal hydraulic theory. Generally, the comparisons are excellent. However, there are often portions of the flow where boundary-layer separation, non-hydrostatic pressures, internal hydraulic jumps, mixing between the layers, and friction are important. In these cases the basic assumptions are violated and internal hydraulic theory does not provide accurate predictions. It is often the case that the theory provides accurate predictions in one portion of the flow but not in another.

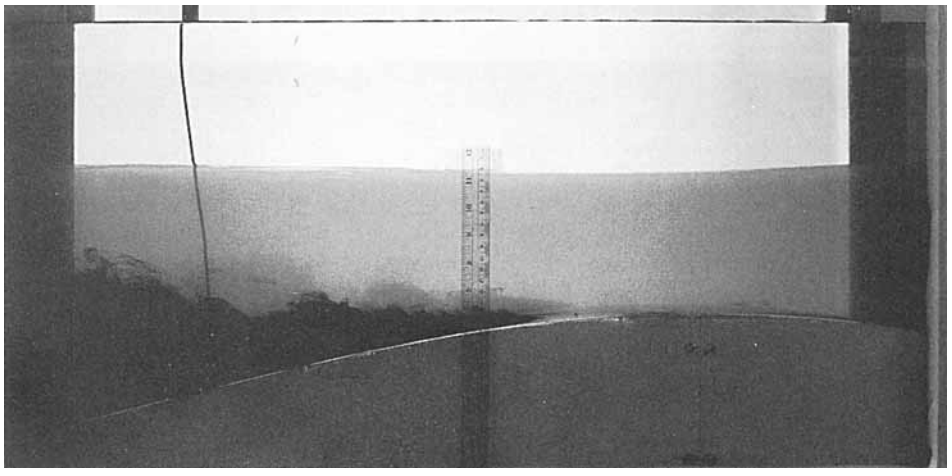

FIGURE 10. Boundary-layer separation downstream of the crest in experiment 25. Flow is from right to left. The separated region appears black from dye injected through the tube visible downstream of the crest.

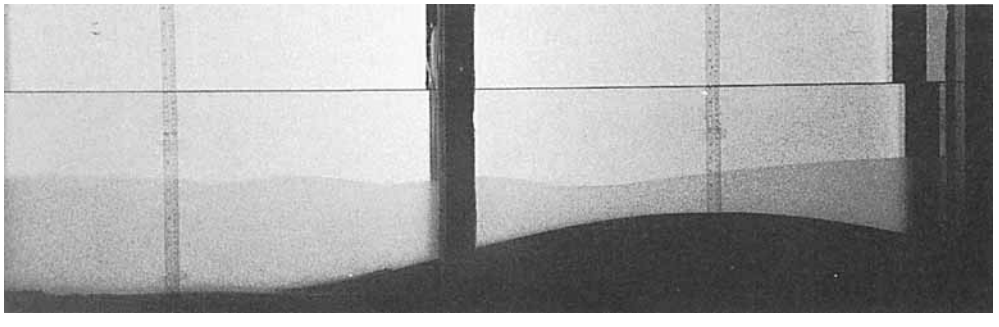

FIGURE 11. Photograph of experiment 2 showing the presence of lee waves. Flow is right to left.

Examples from each flow regime will be discussed to illustrate the circumstances under which internal hydraulic theory is, and is not, appropriate.

5.1. *Regime I: Subcritical flow*

The (E, η)-curves and photograph of experiment 1 presented in figure 7(*a*) provide an example of Regime I (Subcritical flow). Sections 1 and 3 in figure 7(*a*) represent the flow upstream and downstream of the obstacle respectively. They both fall on the subcritical limb of the channel curve. Point 2 representing flow at the crest is on the subcritical limb of the crest curve. The path 1–2–3 is particularly simple, since the flow is subcritical throughout. There is a slight depression in the interface level and a small frictional reduction in internal energy as the flow passes over the obstacle.

The photograph of experiment 1 (figure 7*a*) reveals that the point of maximum depression is downstream of the crest of the obstacle. Downstream of the crest the lower layer diverges and decelerates, causing an adverse piezometric pressure gradient that may result in boundary-layer separation. Figure 10 is a photograph of experiment 25 in which separation has been visualized by injecting dye into the lower layer

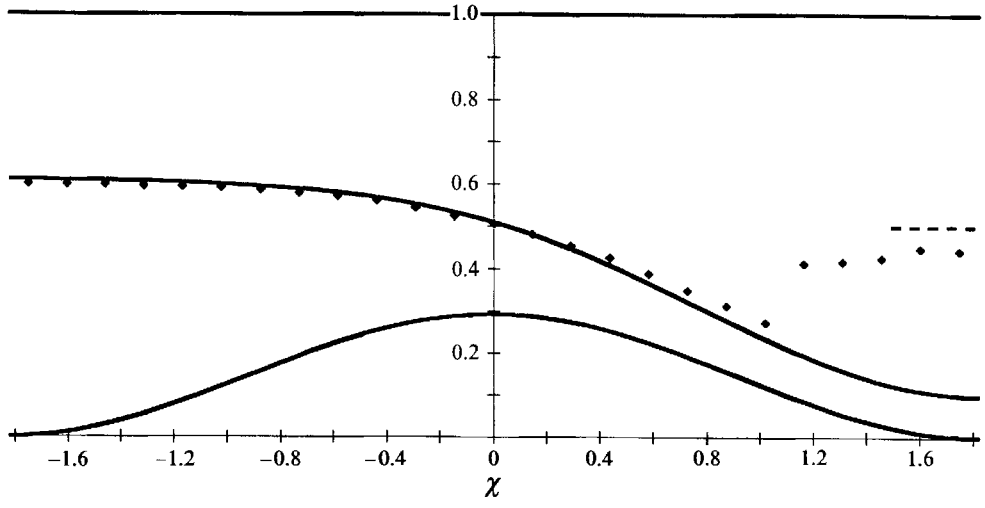

FIGURE 12. Comparison of the predicted longitudinal variation in interface height in experiment 15 with experimental measurements. Flow is left to right.

downstream of the separation point. Given that when the flow separates there is flow reversal in the lower layer, the one-dimensional assumption that the velocity varies only in the flow direction is violated, and we can expect internal hydraulic theory to be compromised. As a result of this (and non-hydrostatic pressures) the flow is not symmetric about the crest as internal hydraulic theory would predict. Separation in two-layer flow over an obstacle is discussed further in Huppert & Britter (1982), Jirka (1984), Lawrence (1984), and in §5.4.

For flows near the boundary between Regimes I and II the asymmetry of the flow becomes more pronounced until a series of lee waves (called an undular jump in the hydraulics literature) forms downstream of the crest, as shown in the photograph of experiment 2 (figure 11). These lee waves are a non-hydrostatic phenomenon and as such are not described by internal hydraulic theory.

5.2. *Regime II: Crest-controlled flow*

Experiment 4, depicted in figure 7(*b*), is an example of Regime II (Crest-controlled flow). Without the obstacle in place, $u_1 = u_2$ and $E = 0$. Unlike subcritical flows, no steady flow solution with this internal energy exists, since $E_c > 0$. With the obstacle in place choking (upstream influence) occurs raising the level of the interface upstream of the obstacle, until the internal energy increases to E_c. The flow can then pass over the obstacle along the path (1–2–3) shown on figure 7(*b*). Downstream of section 3 an internal hydraulic jump forms to match the subcritical condition imposed downstream (section 4). The flow upstream of the obstacle is governed by frictional effects, i.e. a frictional backwater curve. If the backwater curve is allowed to extend far enough upstream the interface will return to its undisturbed level ($\eta = 0$).

A test of the validity of internal hydraulic theory in predicting the longitudinal variation of interface height is provided by experiment 15 shown in figure 12. The predicted interface variation, obtained from (8) and (9), is plotted in figure 12 together with the experimental results. The predicted and measured interface heights agree extremely well, except just upstream of the internal hydraulic jump where the interface level is slightly higher than predicted. Besides experimental error, there are several

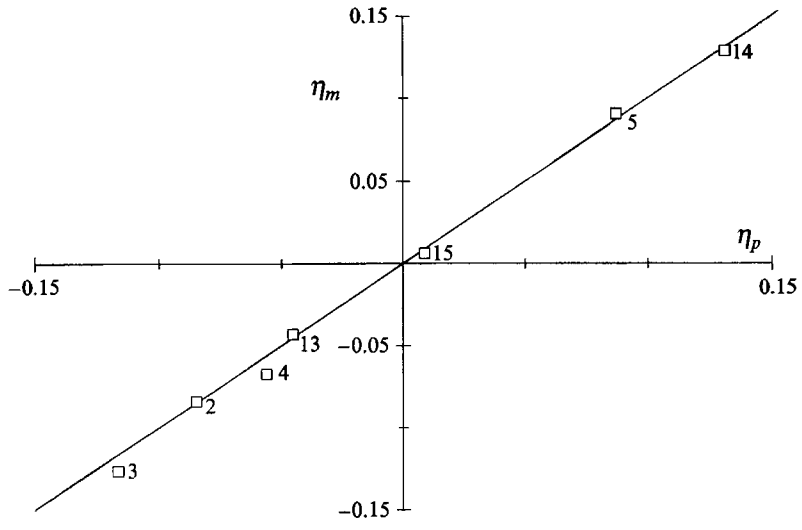

FIGURE 13. Comparison of experimental measurements of interfacial elevation at the crest with predictions for all the crest-controlled flows.

possible reasons for this. Firstly, the internal hydraulic jump blocks flow in the lower portion of the upper layer causing a considerable velocity variation with depth in the upper layer, as in figure 5. Secondly, as the lower layer accelerates, the shear between the two layers causes shear instabilities and mixing between the two layers, see figure 6(*a*). In addition, there may be some non-hydrostatic effects due to streamline curvature.

The validity of internal hydraulic theory in predicting the interfacial elevation at the crest is illustrated in figure 13. There is very good agreement between the predicted and measured interface deflection in each of the seven crest-controlled flows, since $dE/dx \approx 0$ at the crest. The predicted values are obtained by taking the smallest positive solution to the condition of critical flow ($G^2 = 1$) at the crest.

5.3. *Regime III: Approach-controlled flow*

Experiment 7, depicted in figure 7(*c*) is an example of Regime III (Approach-controlled flow), which, unlike the other three regimes, has no counterpart in single-layer flow. It is therefore far less well understood than the other three flow regimes. Approach-controlled flow corresponds to region B′ in Houghton & Isaacson's (1970) numerical study of impulsively started two-layer flow over an obstacle. They found upstream rarefactions, and did not observe the flow asymptoting to a steady state. Similarly, approach-controlled flow corresponds to the flow type E of Baines (1984), who shows that in towing tanks such flows are always accompanied by upstream rarefactions. As discussed in § 1 these rarefactions do not fully develop in the limited length of a towing tank, so steady flow is generally not achieved. The fixed-obstacle experiments of the present study are probably the first to achieve steady Approach-controlled flow.

Approach-controlled flow is similar to Crest-controlled flow in that there is an internal hydraulic control associated with the obstacle, and downstream of the crest there is an internal hydraulic jump. The fundamental difference is that in Approach-controlled flows the internal hydraulic control is located near the foot of the obstacle (the exact position is weakly dependent on frictional forces), not at the crest. Between

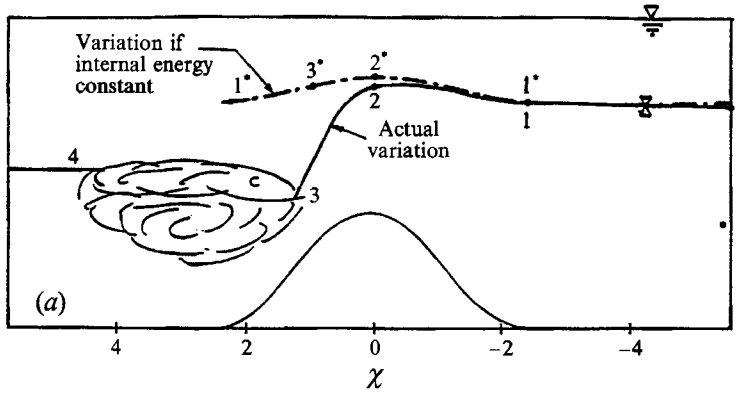

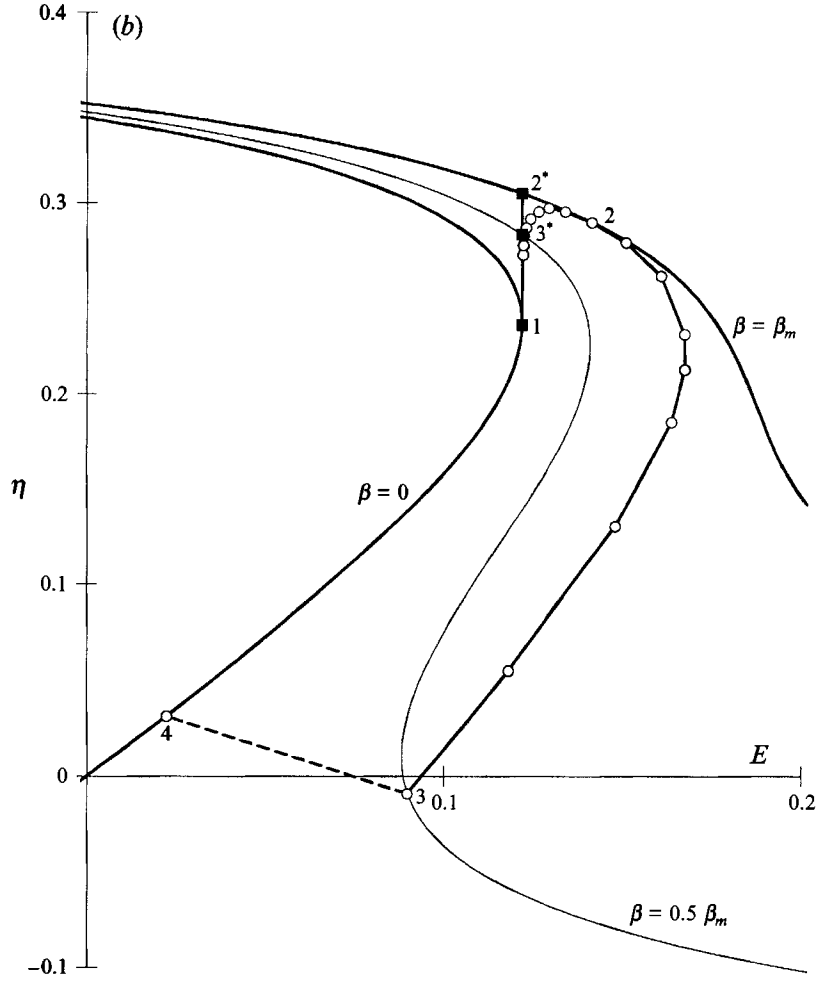

FIGURE 14. (*a*) Experimental variation in interface height in experiment 17, and the variation predicted assuming internal energy conservation. (*b*) Energy diagram for experiment 17 showing the variation in internal energy as the flow passes over the obstacle. The actual flow path (1–2–3–4) is significantly different from the flow path (1–2*–3*–1) that might have occurred if internal energy remained constant.

the Approach control and the crest the interface rises approximately in accordance with (8). However, downstream of the crest the interface plunges rapidly; this behaviour cannot be explained using internal hydraulic theory, since the internal energy varies dramatically just downstream of the crest, see figures 7(*c*) and 14(*b*).

5.3.1. *Importance of flow curvature*

Experiment 17, see figures 6(*c*) and 14(*a*), was performed to examine the effects of the variation in internal energy in greater detail. The (E, η)-diagram for this experiment is presented in figure 14(*b*). Lawrence (1985) has shown that the variation in internal energy as the flow passes over the sill is far more rapid than can be attributed to frictional effects. At the crest there is an increase in internal energy as a result of significant streamline curvature. From (4) we see that the convex flow will reduce the piezometric pressure in the lower layer more than in the upper layer. By assuming hydrostatic flow we will overestimate E_2 more than E_1, so from (10), the internal energy (calculated on the assumption of hydrostatic flow), will increase. This situation reverses on the lee side of the obstacle when the flow changes curvature. An important experimental observation is that downstream of the crest the interface falls slightly at first and then plunges rapidly. Across this 'supercritical leap' the flow changes from one that is supercritical with $F_1^2 \gg F_2^2$ (i.e. an 'active' upper layer in the terminology of Armi 1986), to one that is supercritical with $F_2^2 \gg F_1^2$ (i.e. an active lower layer). Once the lower layer is the active layer the flow can jump (at section 3) to match the subcritical condition imposed downstream (section 4). The loss of internal energy in the internal hydraulic jump is consistent with the observation that turbulent dissipation occurs almost exclusively in the lower layer, see Wood & Simpson (1984).

If the internal energy were to have remained constant over the obstacle the flow would have had to follow the path 1–2*–3*–1 on figure 14(*a*). Long (1954) hypothesized that a form of internal hydraulic jump, which he called a 'hydraulic drop', might occur at a point between the crest and the end of the obstacle, say point 3*, causing a thickening of the upper layer to match the subcritical downstream flow. This behaviour is unlikely in steady two-layer flow over an obstacle, since energy would be dissipated primarily in the upper layer, which from (10) would yield an increase in internal energy. From figure 14(*b*) we see that a decrease, not an increase, in internal energy is required to match the downstream condition.

Lawrence (1985) has shown that the term hydraulic drop has been used in the least five contexts by previous investigators. However, all the flows observed in the present study, and all the published photographs of flows in previous studies, can be explained without invoking the presence of a hydraulic drop. For example, in the flows depicted in figures 9 and 12 of Long (1954) there is considerable turbulent activity over the lee face of the obstacle; however, in figure 9 the disturbance originates at the sidewalls, and in figure 12 separation from the lee face of the obstacle occurs. Approach-controlled flows exhibiting separation from the lee face of a steep obstacle are shown in figures 24(*b*), 24(*c*), and 25(*a*) of Baines (1984). Separation does not occur in figure 24(*a*) of Baines (1984), where he uses a much gentler obstacle. In this experiment the interface plunges as in the Approach-controlled flows of the present study.

5.3.2. *Prediction of Approach-controlled flow*

The development of a model to accurately predict the behaviour of Approach-controlled flow as it passes over the obstacle is beyond the scope of the present study. Several investigators including Pite, Topham & van Hardenberg (1992), Marchant &

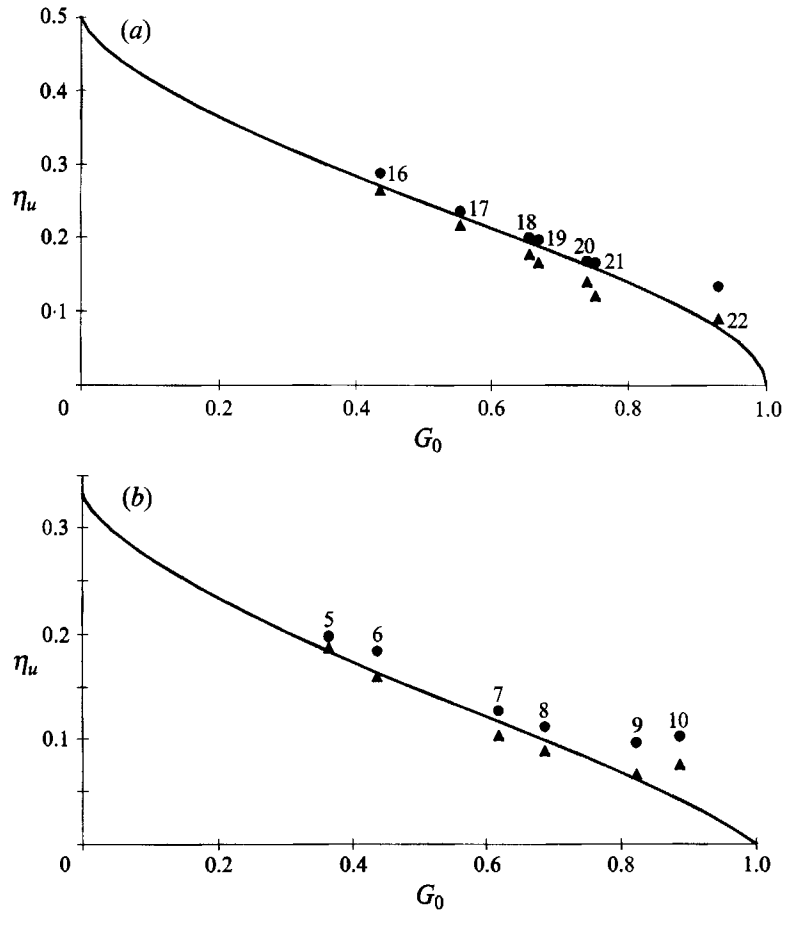

FIGURE 15. Comparison between predicted and measured values of upstream influence for all the approach-controlled flows: (*a*) $r = \frac{1}{2}$, (*b*) $r = \frac{2}{3}$. Measurements made 1 and 2 m upstream of the obstacle are indicated by the symbols ▲ and ● respectively.

Smyth (1990), and Melville & Helfrich (1987) have used the forced extended Korteweg–de Vries (KdV) equation to study transcritical ($G_0 - 1 \ll 1$) flow over an obstacle. In addition to the flow being transcritical, the forced extended KdV equation assumes that the ratio of the flow depth to the obstacle length Y/L, the interface deflection at the approach-control (upstream influence) η_u, and the relative height of the obstacle β_m, are all small. Unfortunately, these conditions do not apply in the present study. For the Approach-controlled flows of the present study

$$0.17 \leqslant 1 - G_0 \leqslant 0.64,\ 0.44 \leqslant Y/L \leqslant 0.87,\ 0.066 \leqslant \eta_u \leqslant 0.287, \text{ and } 0.30 \leqslant \beta_m \leqslant 0.57.$$

Two-layer flow over a towed obstacle has been modelled numerically with considerable success by Jameel (1991) using a two-dimensional model based on the Marker and Cell technique of Harlow & Welch (1965). This technique will be investigated in future modelling of Approach-controlled flows over a fixed obstacle, but for the moment some useful results obtained using internal hydraulic theory will be presented.

Despite the importance of flow curvature elsewhere in Approach-controlled flows, it is important to note that there is negligible curvature at the approach-control itself, so

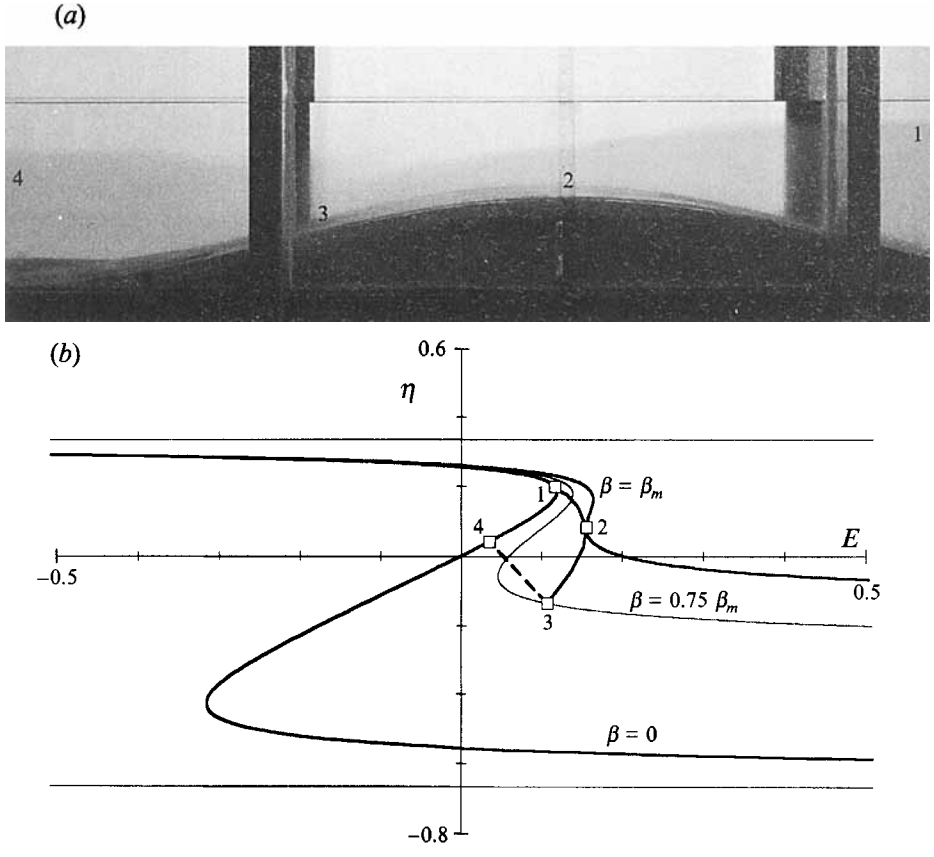

FIGURE 16. Photograph and internal energy diagram for experiment 5, a hybrid flow with both an approach control (point 1) and a crest control (point 2).

internal hydraulic theory ought to apply there. The upstream influence, η_u, is calculated from the condition of critical flow at the approach control, which, for $r = 0.5$, yields

$$\xi^3 - 3\xi^2 + 3(2G_0^2 + 1)\xi + (2G_0^2 - 1) = 0, \tag{16}$$

where $\xi = (\eta_u/r)^2$. There is one real root and two complex conjugate roots to this equation. The real root is

$$\xi = 1 - (2G_0^2)^{\frac{1}{3}}\{[(1 + G_0^2/4)^{\frac{1}{2}} + 1]^{\frac{1}{3}} - [(1 + G_0^2/4)^{\frac{1}{2}} - 1]^{\frac{1}{3}}\}. \tag{17}$$

This equation is used to obtain the theoretical values of upstream influence that are plotted on figure 15(*a*) together with the measured interface deflections both 1 and 2 m upstream of the crest of the obstacle for all of the Approach-controlled experiments. Measurements were taken at both locations, since the interface elevation is slowly changing as a result of friction between the layers and along the bottom and sidewalls of the channel. It is these frictional effects that determine the exact location of the control. The results show that for all the experiments, except experiment 22, the approach-control is between 1 and 2 m upstream of the crest of the obstacle.

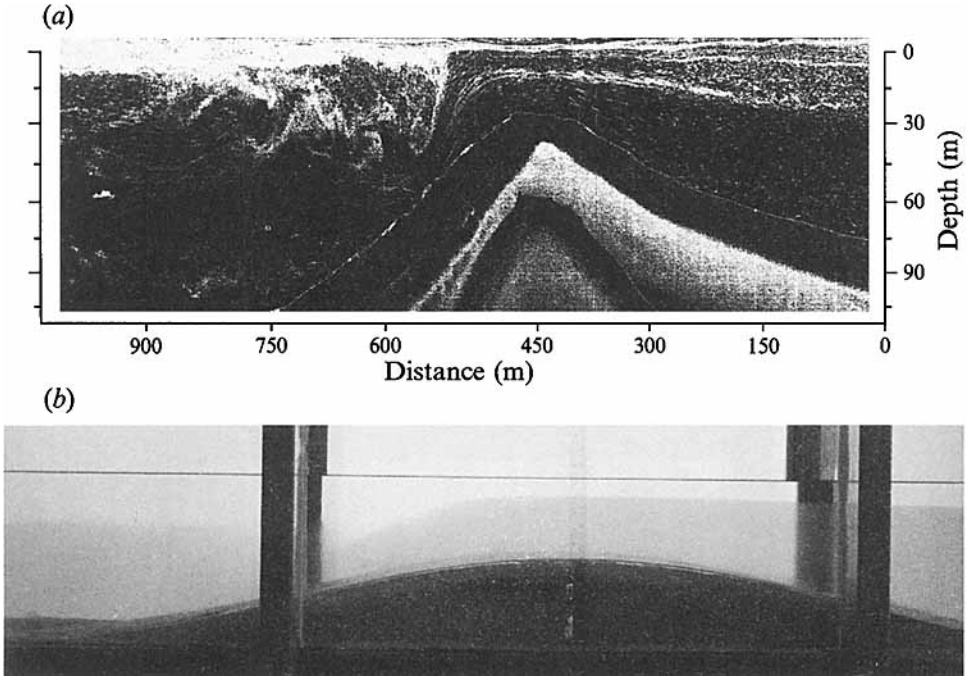

FIGURE 17. Two comparable approach-controlled flows. (*a*) An acoustic image of the flow over the sill in Observatory Inlet, British Columbia (from Farmer & Denton 1985, figure 4). Note that the horizontal scale has been compressed. (*b*) Photograph of experiment 6; a scaled down approximation to the flow depicted in (*a*). Flow is from right to left in both cases.

5.3.3. *Hybrid flows*

Experiment 22 is a special case, since it lies close to the boundary separating Approach-controlled flow from Supercritical flow in the classification diagram (figure 8*b*). In fact, it is a hybrid flow that behaves like an Approach-controlled flow, except that it is supercritical upstream of the obstacle. The reason for this behaviour is that for flows with G_0 approaching unity the small change in internal energy caused by frictional effects can be important over the 12.8 m length of the flume. This enables the flow to be supercritical as it enters the flume and subcritical as it exits, independent of whether there is an obstacle in the flume or not. This is evidenced by the fact that when the obstacle was removed in experiment 22 an undular jump formed in the channel to provide a transition from supercritical to subcritical flow.

For $r \neq \frac{1}{2}$, η_u must be calculated numerically. The results for $r = \frac{2}{3}$ are plotted on figure 15(*b*) together with experimental measurements. Again the approach control is between 1 and 2 m upstream of the crest, except for a hybrid flow, experiment 10. For both $r = \frac{1}{2}$ and $\frac{2}{3}$ hybrid flows occur near the boundary between Approach-controlled and Supercritical flows in the classification scheme, as we would expect.

Hybrid flows also exist that combine feature of both Crest-controlled and Approach-controlled flows; experiment 5 is an example of this. Figure 13 shows that the flow is critical at the crest and figure 15(*a*) shows that the flow is also critical at a point approximately 2 m upstream of the crest of the obstacle. This observation is supported by the (E, η)-plot for this experiment (figure 16*b*). The internal energy increases from E_a just upstream of the obstacle, to E_c at the crest. Although this flow has an approach control, the interface level decreases on the upstream face of the obstacle like a Crest-

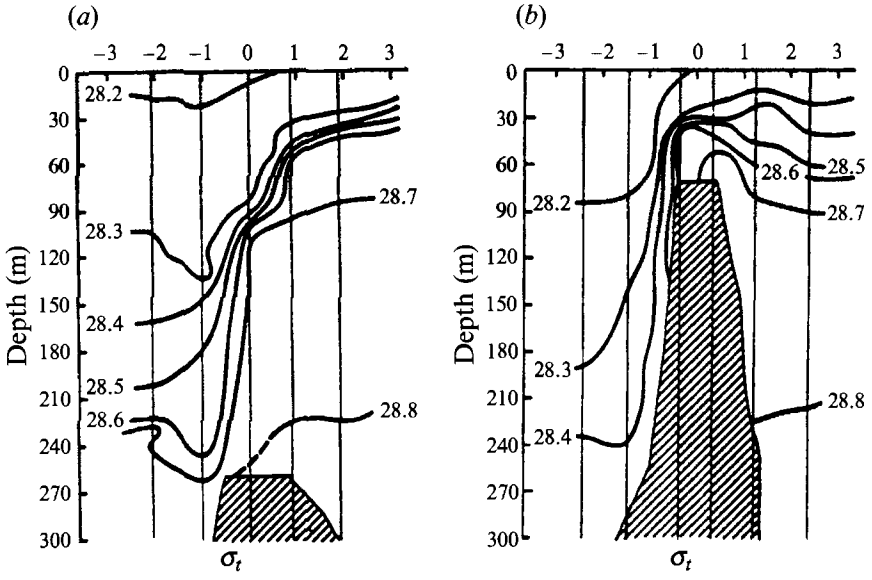

FIGURE 18. Isopycnals in: (*a*) Enterprise Passage, where the interface falls as it flows toward the crest, indicating crest-controlled flow; and (*b*) Grafton Passage, where the interface rises as it flows toward the crest, indicating approach-controlled flow. Density is measured in σ_t units, where $\rho(\sigma_t) = \rho(kg/m^3) - 1000$. North is to the right. From Murray *et al.* (1984, figure 10).

controlled flow (see figure 16*a*). Clearly this type of hybrid flow is limited to situations where the (E, η)-curve at the crest has a local minimum corresponding to critical flow. From (14) this only occurs if

$$G_0^2 < \frac{(1-\beta_m)^3}{r(1-r)[r^{\frac{1}{2}}+(1-r)^{\frac{1}{2}}]^4}. \tag{18}$$

On the basis of (18) experiment 5 should be the only experiment in the present study exhibiting features of both Crest-controlled and Approach-controlled flow. This is indeed the case.

5.3.4. *Field observations of Approach-controlled flows*

An acoustic image of flow over a sill in Observatory Inlet, British Columbia is presented in figure 17(*a*). The presence of acoustic reflectors in the water column ensures that this image provides a qualitative picture of the flow field. The features of an Approach-controlled flow are evident. The interface plunges downstream of the crest and then returns to an internally subcritical state via an internal hydraulic jump. Since the time taken for the flow to pass over the sill is only of the order of ten minutes Farmer & Denton (1985) assume that the flow is steady. They also assume that it is two-dimensional and three layered with a thin passive upper layer. Their representation of the flow gives $r = 0.6$, $\beta_m = 0.6$, and $G_0 = 0.5$ for the flow of the lower two layers. Of the experiments performed in the present study the one that comes closest to these values is experiment 6 ($r = 0.66$, $\beta_m = 0.57$, and $G_0 = 0.44$) shown in figure 17(*b*). Given the compression of the horizontal scale in figure 17(*a*), the similarity between the two flows is remarkable. Farmer & Denton (1985) hypothesize that the plunging of the interface in Observatory Inlet is due to an inverted hydraulic jump or a so-called 'hydraulic drop'; this is not the case in experiment 6 and is unlikely to be the case in Observatory Inlet.

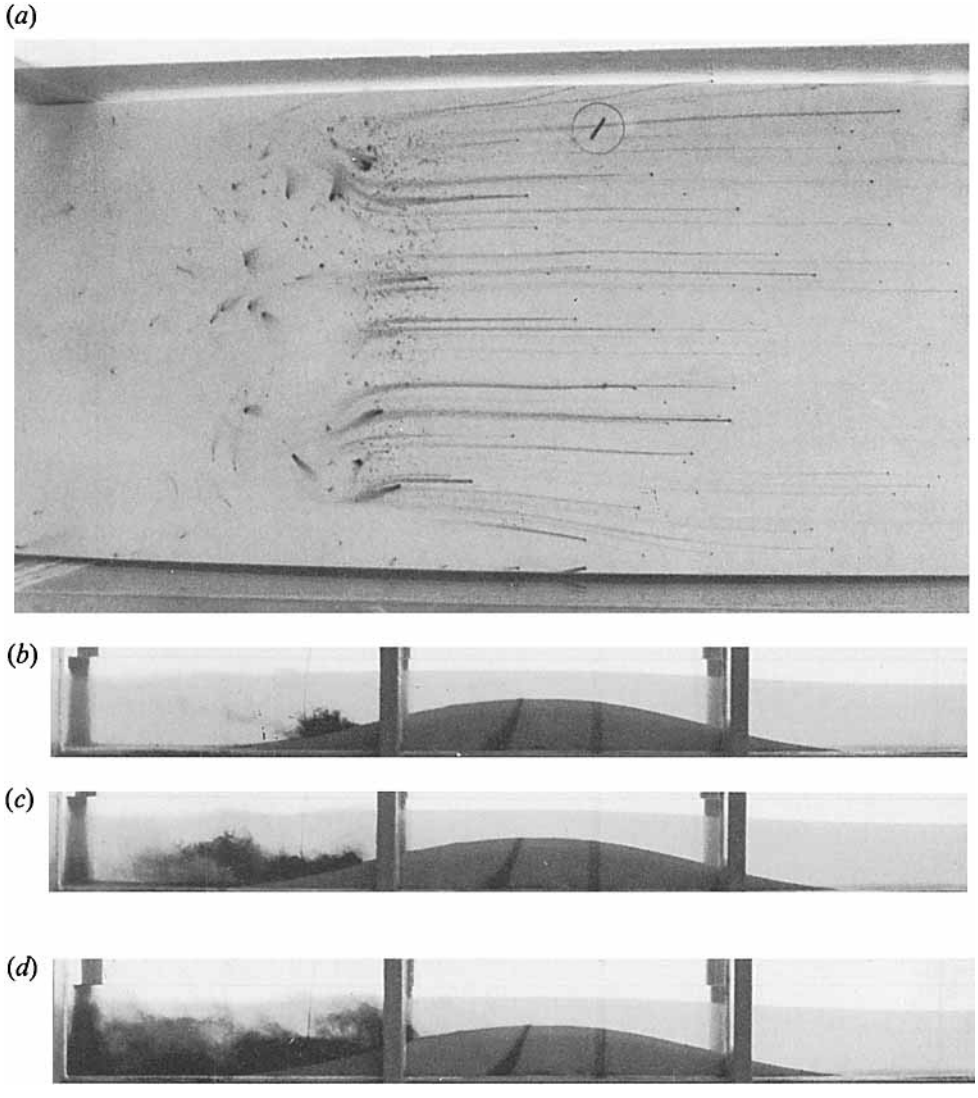

FIGURE 19. Photographs of experiment 12 showing separation in a Supercritical flow. (*a*) Plan view from above the obstacle in experiment 12. Dye particles have been dropped into the flow. In regions of unseparated flow these particles rest on the sill and produces long streaklines as they dissolve. The streaklines are disrupted as soon as they enter regions of flow separation. (*b–d*) Photographs taken at 10 s intervals after the injection of dye onto the lee face of the sill. Boundary-layer separation is vigorous enough to mix the injected fluid over the depth of the lower layer, and even cause some mixing at the interface.

Further evidence of Approach-controlled flow is provided by the plots of flow over sills in the Tiran Strait between the Gulf of Aqaba and the Red Sea by Murray, Hecht & Babcock (1984, figure 10). The flow in Enterprise Passage (figure 18*a*) is an exchange flow that appears to be critical at the crest. In the Grafton Passage (figure 18*b*) the flow is unidirectional, and, therefore, of less interest from the point of view of exchange between the Red Sea and the Gulf of Aqaba; however, it appears to be an example of Approach-controlled flow, since the interface remains almost horizontal until beyond the crest where it plunges rapidly.

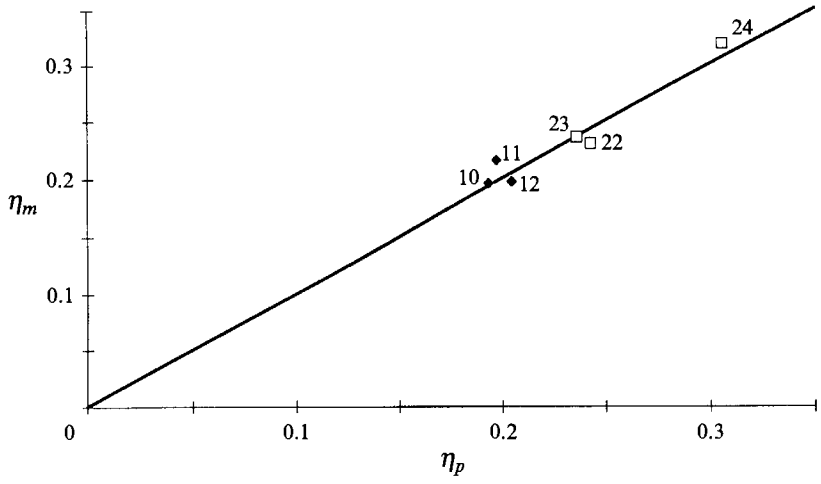

FIGURE 20. Comparison of experimental measurements of interfacial elevation at the crest with predictions for all the Supercritical flows. ◆, Experiments with $r = \frac{2}{3}$; □, experiments with $r = \frac{1}{2}$.

5.4. *Regime IV: Supercritical flow*

Experiment 12, depicted in figure 7(*d*), is an example of Supercritical flow. Since $G_0^2 > 1$ a virtual control occurs in the upstream contraction and the flow is internally supercritical as it enters the flume. The flow remains supercritical as it passes through the flume and over the obstacle. Downstream of the obstacle the lower layer diverges causing an adverse piezometric pressure gradient that results in boundary-layer separation. This is demonstrated in the series of photographs presented in figure 19. In photograph 19(*a*), taken from above the flume, dye particles have been dropped into the flow. In regions of unseparated flow these particles rest on the sill, and produce long streaklines as they dissolve. Particles resting on the sill in the region of flow separation produce no streaklines, since the flow is continually changing direction. Note that the sidewall boundary layers separate before the bottom boundary layer. Photographs 19(*b–d*) were taken at 10 second intervals after the injection of dye onto the lee face of the sill. They show that the boundary-layer separation is vigorous enough to mix the injected fluid throughout the lower layer, and even cause some mixing at the interface.

Even if there is flow separation it should not affect the flow at the crest. Figure 20 shows that the predicted interface elevation at the crest is in excellent agreement with the measured value for each of the four Supercritical flows (experiments 11, 12, 23 and 24) and for the two hybrid flows combining features of Approach-controlled and Supercritical flow (experiments 10 and 22). The predicted values are obtained by solving (12) with $E = 0$ and $\beta = \beta_m$.

6. Conclusions

The finite length of towing-tank facilities sometimes limits their applicability for the study of steady two-layer flow over an obstacle. This is particularly true in the case of Approach-controlled flows. Careful study of the variation of interface level in fixed-obstacle experiments has provided a more complete understanding of Approach-controlled flows. These flows pass from being internally subcritical to being internally supercritical (with an active upper layer) at a control located just upstream of the start of the obstacle. As the flow passes over the obstacle the upper layer remains active until

downstream of the crest where the interface plunges rapidly resulting in an internally supercritical flow with an active lower layer. Further downstream an internal hydraulic jump transforms the flow back to an internally subcritical state. The plunging of the interface in Approach-controlled flows is explained by considering streamline curvatures, and the corresponding non-hydrostatic pressures. It is not necessary to invoke a shock solution (called an internal hydraulic drop by previous investigators) to explain the plunging of the interface.

The importance of non-hydrostatic pressures is of some concern, since the hydrostatic assumption is fundamental to hydraulic theory. Fortunately, however, non-hydrostatic pressures are not significant in the vicinity of internal hydraulic controls. So the validity of a classification scheme derived on the basis of being able to predict when and where internal hydraulic controls occur is not compromised. This classification scheme accurately predicts when each of the four basic steady flow regimes (Subcritical, Crest-controlled, Approach-controlled and Supercritical flow) will occur.

I am deeply grateful to Gilles Corcos and the late Hugo Fischer for providing the inspiration to pursue this study; and to Larry Armi, Johannes Buhler, Hubert Burnett, Richard Denton, David Farmer, Stephen Monismith, Catherine van Ingen and Carlos White for the considerable help they provided at various stages of this study. This research was funded by the US National Science Foundation and the Canadian Natural Sciences and Engineering Research Council. I also received the support of a Hackett Overseas Studentship from the University of Western Australia, and a Hans Albert Einstein Memorial Fellowship from the University of California at Berkeley.

Appendix. Symbols and definitions

$Y = y_1 + y_2 + h$	free surface elevation
y_n	layer thickness ($n = 1$ or 2)
$y_{2o} = rY$	lower-layer thickness when $u_1 = u_2$
E_n	layer mechanical energy per unit volume (Bernoulli constant)
$F_n^2 = u_n^2/g'y_n$	densimetric Froude number
g	gravitational acceleration
g'	reduced gravitational acceleration
h	obstacle height
h_m	maximum obstacle height
$G^2 = F_1^2 + F_2^2$	composite Froude number
G_0^2	composite Froude number when $u_1 = u_2$
P	pressure
$P^* = P + \rho gz$	piezometric pressure
q_n	layer flow rate
$q = q_1 + q_2$	total flow rate
$r = q_2/q$	flow rate ratio
$u_n = q_n/y_n$	layer velocity
$\beta = h/Y$	obstacle height (dimensionless)
$\beta_m = h_m/Y$	maximum obstacle height (dimensionless)
$\chi = x/Y$	horizontal position (dimensionless)
$\epsilon = (\rho_2 - \rho_1)/\rho_2$	relative density difference
E	internal energy (dimensionless)
E_c	internal energy at a crest control

E_a	internal energy at an approach control
$\eta = (h+y_2-y_{2o})/Y$	interface deflection (dimensionless)
η_u	upstream influence – the interface deflection upstream of the obstacle
η_m	measured interface deflection
η_p	predicted interface deflection
ρ	fluid density

Subscripts

$n = 1$	upper layer
$n = 2$	lower layer

REFERENCES

ARMI, L. 1986 The hydraulics of two flowing layers of different densities. *J. Fluid Mech.* **163**, 27.

BAINES, P. G. 1984 A unified description of two-layer flow over topography. *J. Fluid Mech.* **146**, 127.

BAINES, P. G. 1987 Upstream blocking and airflow over mountains. *Ann. Rev. Fluid Mech.* **19**, 75.

DALZIEL, S. B. 1990 Two-layer hydraulics: a functional approach. *J. Fluid Mech.* **223**, 135.

DENTON, R. A. 1987 Locating and identifying hydraulic controls for layered flow through an obstruction. *J. Hydraul. Res.* **25**, 281.

FARMER, D. M. & DENTON, R. A. 1985 Hydraulic control of flow over the sill in Observatory Inlet. *J. Geophys. Res.* **90(C5)**, 9051.

FARMER, D. M. & FREELAND, H. J. 1983 The physical oceanography of fjords. *Prog. Oceanogr.* **12**, 147.

FARMER, D. M. & SMITH, J. D. 1980 Tidal interaction of stratified flow with a sill in Knight Inlet. *Deep-Sea Res.* **17**, 239.

HARLOW, F. H. & WELCH, J. E. 1965 Calculation of time-dependent viscous incompressible flow of fluid with a free surface. *Phys. Fluids* **8**, 2182.

HENDERSON, F. M. 1966 *Open Channel Flow*. MacMillan.

HOUGHTON, D. D. & ISAACSON, E. 1970 Mountain winds. *Stud. Numer. Anal.* **2**, 21.

HUPPERT, H. E. & BRITTER, R. E. 1982 Separation of hydraulic flow over topography. *J. Hydraul. Engng* **108**, 1532.

JAMEEL, M. I. 1991 Modelling of two-layer flow over an obstacle. PhD thesis, Department of Mechanical Engineering, University of Calgary.

JIRKA, G. H. 1984 Discussion of 'Separation of hydraulic flow over topography' by Huppert & Britter (1982). *J. Hydraul. Engng* **110**, 357.

LAWRENCE, G. A. 1984 Discussion of 'Separation of hydraulic flow over topography' by Huppert & Britter (1982). *J. Hydraul. Engng* **110**, 359.

LAWRENCE, G. A. 1985 The hydraulics and mixing of two-layer flow over an obstacle. PhD thesis, Department of Civil Engineering, University of California, Berkeley.

LAWRENCE, G. A. 1987 Steady flow over an obstacle. *J. Hydraul. Engng* **113**, 981.

LAWRENCE, G. A. 1990 On the hydraulics of Boussinesq and non-Boussinesq two-layer flows. *J. Fluid Mech.* **215**, 457.

LONG, R. R. 1954 Some aspects of the flow of stratified fluids. II. Experiments with a two-fluid system. *Tellus* **6**, 97.

MARCHANT, T. R. & SMYTH, N. F. 1990 The extended Korteweg–de Vries equation and the resonant flow of a fluid over topography. *J. Fluid Mech.* **221**, 263.

MELVILLE, W. K. & HELFRICH, K. R. 1987 Transcritical two-layer flow over topography. *J. Fluid Mech.* **178**, 31.

MURRAY, S. P., HECHT, A. & BABCOCK, A. 1983 On the mean flow in the Tiran Strait in winter. *J. Mar. Res.* **42**, 265.

PITE, H. D., TOPHAM, D. R. & HARDENBERG, B. J. VAN 1992 Laboratory measurements of the drag force on two-dimensional topographic features in a two-layer flow. *J. Fluid Mech.* (submitted).

US ARMY CORPS OF ENGINEERS 1980 *Hydraulic Model Study for the John F. Baldwin Ship Channel – Incremental Improvements with/without Fluid Submerged Barriers.* Department of the Army, San Francisco, CA, July 1980.

WOOD, I. R. 1968 Selective withdrawal from a stably stratified fluid. *J. Fluid Mech.* **32**, 209.

WOOD, I. R. & SIMPSON, J. E. 1984 Jumps in layered miscible fluids. *J. Fluid Mech.* **140**, 329.